τ	7	1	averaging	CC 4	•	1.		C	r 1	1	C 1	1
1	$^{\prime}$	liime	averaging	ettect	in non	linear	nrocesses	α t 1	tocused	lacer	tiel	de
•	U	Tullic	averaging	CIICCU	111 11011	mcai	processes	\mathbf{OI}	locuscu	lasel	1101	us

Yuzhong Yao, William M. Freund, Jie Zhang, and Wei Kong*

Department of Chemistry, Oregon State University, Corvallis, OR 97331-4003

Manuscript for submission to J. Chem. Phys., Experimental methods, 5/17/2021

^{*}Corresponding author, wei.kong@oregonstate.edu

Abstract

We report theoretical derivations and experimental results on the volume averaging effect of nonlinear processes in focused laser fields. This effect is considered detrimental in revealing the intensity dependence of a nonlinear process, caused by the intensity variation across the sampled volume of a focused laser. Following the treatment in the literature, we prove that if the signal dependence can be expressed as a simple power function of the laser intensity and if the detection region encompasses effectively the whole volume, volume average does not affect the final conclusion on the derived exponent. However, to reveal the detailed saturation effect of a multi-photon process, intensity selective scans involving spatial filters and displacement of the laser focus (z-scan) are required. Moreover, to fully capture the dependence of the signal on the variation of the laser intensity, the degree of spatial discrimination and the corresponding range of z-scan need to be modeled carefully. Limitations in the dynamic range of the detector or the laser power, however, can thwart the desired scan range, resulting in erroneous fitting exponents. Using our nanosecond laser with a non-ideal Gaussian beam profile, based on multiphoton ionization of argon atoms from a collimated molecular beam and from ambient argon gas, we report experimental measurements of the beam waist and Rayleigh range, and compare the experimental intensity dependence of Ar⁺ with theoretical values. Agreements between theory and experiment are remarkable.

Introduction

In nonlinear optical processes using focused laser beams, typically the sample volume is larger than the focal volume of the laser beam, as shown in Fig. 1. The detected responses from the interaction region, consequently, can encompass contributions from the entire sampled volume, including the volume that is outside the focal volume of the laser. The result is therefore considered an average within the volume of interaction. This volume average effect (VAE) is prevalent in both gas phase and condensed phase experiments, and it is considered detrimental for quantitative characterizations of the effect of the laser intensity. 1-5 In pump-probe experiments, 6 fortunately, this problem is irrelevant because the overlapping beams can typically select the volume of interaction, confining the experiment to a fixed volume.

To circumvent VAE, methods of discrimination of either the sample volume or the sampled volume, i.e., spatial filters, have been implemented. In the first approach, a small tube is used to limit the spread of the molecular beam in the interaction region, with the tube diameter comparable to the Rayleigh range (z_0) of a Gaussian beam. In the second approach, a slit aperture is used to choose ions from only a small section – again comparable to the Rayleigh range – along the propagation direction of the laser (designated as the z direction). In both cases, the pulse energy of the laser beam is kept constant, but the focus of the laser beam is shifted along the z direction. The resulting signal is considered an average across the laser beam along the radial (r) direction, but with no average along the propagation direction. Further treatments of the results can then reveal the true intensity dependence function, z_0 i.e. the response function z_0 , where z_0 is the intensity of the laser beam. Both methods are collectively called z_0 -scan, and the experiment is termed intensity selective scanning (ISS) in the literature.

The derivation of R(I) from experiments of z-scan requires information on the properties of the laser beam along both the r and z directions. For ideal Gaussian beams, detailed mathematical treatments have been reported, 2,3 and the method has been used in studies of Coulomb explosions in strong fields using femtosecond lasers. 5,8 However, for non-ideal Gaussian beams, such as those from typical nanosecond lasers, a detailed characterization of the laser beam is necessary. Recently several groups including us have observed multiply charged atomic ions from interactions between a focused nanosecond laser beam and a cluster beam, $^{9-11}$ and the need to solve the VAE for non-ideal Gaussian beams becomes imperative.

In this work, we present a few relatively straightforward solutions to the VAE problem for both ideal and non-ideal Gaussian beams. We will review the treatment of ideal Gaussian beams² and introduce a few short-cuts in deriving the volume independent signal when the signal dependence can be simplified into a power function of the laser intensity. We have also characterized our nanosecond laser beam, and will report the experimental results on the beam waist and Rayleigh range. Using multiphoton ionization of Ar at 532 nm, we will demonstrate the effectiveness of the short-cuts in deriving the volume independent signal and thereby the dependence of the ionization yield on the laser intensity. We also present a caveat in performing ISS experiments with methods of spatial discrimination: when the width of the slot or the tube is comparable to the Rayleigh range, the scanning range needs to exceed $2z_0$ to reveal the true exponent.

Ideal Gaussian beams

For an ideal focused Gaussian beam, the beam intensity is represented by:²

$$I(z,r) = \frac{I_0}{1 + (\frac{z}{z_0})^2} e^{-\frac{r^2}{w(z)^2}},$$
(1)

where

$$w(z)^{2} = w_{0}^{2} \left(1 + \left(\frac{z}{z_{0}} \right)^{2} \right), \tag{2}$$

and

$$z_0 = \frac{\pi w_0^2}{\lambda}.\tag{3}$$

In these equations, λ is the wavelength of the laser, w_0 is the smallest beam waist at the focal position, I_0 is the intensity at the focal spot, r is the radial displacement from the center of the beam, and z is the distance from the focal position.

In an ionization experiment, the detected signal should be directly proportional to the response function R(I), where I is dependent on the position (z,r). Following the notation of ref. ², without spatial discrimination in the detection scheme, the signal S_{FV} is considered from the full-view, while the signal from ISS experiments is designated as S_{ISS} . After introducing an integration kernel in each case, the detected signal can be expressed as:

$$S_{FV}(z) = \frac{1}{3}\rho\pi w_0^2 z_0 \int_0^{I_0} \frac{2I + I_0}{I^2} \left[\frac{I_0 - I}{I} \right]^{1/2} R(I) dI, \tag{4}$$

$$S_{ISS}(z) = \frac{1}{2} \rho \pi w_0^2 \Delta z \frac{I_0}{I_{0L}(z)} \int_0^{I_{0L}(z)} \frac{R(I)}{I} dI,$$
 (5)

Where ρ is the particle density – considered uniform across the interaction volume, $I_{0L}(z)$ is the axial intensity of the laser beam, i.e. intensity along the optical axis with r = 0 according to Eq. 1, and Δz is the width of the collection slot or diameter of the tube (Fig. 1). The goal of any experiment on intensity effects is to reveal the functional form of R(I) from the experimental values of S_{FV} or S_{ISS} without the interference of VAE.

In the case of ISS, the derivation of R(I) from Eq. (5) can be obtained from:²

$$R(I) \propto \left(\frac{I_{0L}(z)}{dI_{0L}(z)/dz}\right) \frac{d[I_{0L}(z)S_{ISS}(z)]}{dz},\tag{6}$$

which involves differentiation of the experimental signal with respect to z, achievable using small uniform steps in the z-scan experiment. In the case of full-volume experiments, however, there is no analytical method to derive R(I). For this reason, even though ISS experiments are challenging in alignment because of the spatial filter, they are necessary to reveal the true response function.

On the other hand, in many strong field experiments, we simplify the expression of R(I) as a power function

$$R(I) = cI^n \,, \tag{7}$$

Where c is a proportionality constant, and n is the order of the reaction, typically considered to be related to the number of photons involved in the process. Eq. (7) is applicable when the optical process is either far away from saturation or completely saturated in some steps of a multistep process. In other words, the experimentally derived value n can be considered an indicator for the presence of saturation. When the laser intensity I is comparable to the saturation intensity I_s , a denominator involving $(1 + \frac{I}{I_s})$ for Eq. (7) will complicate the situation immensely.

With this prior knowledge of the functional form of R(I) from Eq. (7), Eq. (5) can be further derived into:

$$S_{ISS}(z) = \frac{1}{2} \rho \pi w_0^2 \Delta z I_0 \frac{c}{n} I_{0L}(z)^{n-1} . \tag{8}$$

Eq. (8) indicates that from a direct fitting of S_{ISS} as a function of I_{0L} , the resulting exponent should be consistently lower than the true exponent by 1. Hence there is no need to perform the differentiation of Eq. (6) in data treatment. Although not a significant reduction in work load, this

simplification is a welcoming relief because the differentiation of Eq. (6) can significantly magnify the experimental uncertainty and result in non-physical values.^{2,7}

Instead of z-scan, we also consider another method of obtaining $S_{ISS}(I)$, i. e. a power-scan: ^{12,13} with the spatial discrimination tube or slot in place to confine the detection volume to the Rayleigh range along the z direction, one can simply scan the power of the laser while monitoring the ion yield. For an ideal Gaussian beam, the beam waist and Rayleigh range are independent of laser intensity. Direct fitting of the signal as a function of the laser intensity should yield the exact exponent of Eq. (7).

Both power scan and z-scan rely on the knowledge of the laser beam. Power scan is only applicable when the beam parameters are independent of pulse energy. In comparison, z-scan uses the same pulse energy, hence its results should not be affected by the variation of beam parameters at different pulse energies. However, z-scan requires the knowledge of the Rayleigh range, a parameter that requires experimental characterization, as will become clear in the following section. Substituting Eq. (7) into Eq. (4) in the full-view experiment, the integration is not easily solvable. However, if we remain in the cylindrical coordinate (r, z), the signal from a full-view experiment can be derived analytically. We first substitute Eq. (1) into Eq. (7) and integrate over the radial direction to obtain the z dependence of the signal $S_r(z; I_0)$:

$$S_r(z; I_0) = \frac{c\pi\rho w_0^2 I_0}{n} I_{0L}(z)^{n-1} . \tag{9}$$

This result is in agreement with Eq. (8) from the ISS experiment, corresponding to the signal recorded from 0 to ∞ in the r direction for the same z value, i. e. ions from a slice with an infinitely large area. The integration of $S_r(z; I_0)$ over z results in $S_{rz}(z; I_0)$:

$$S_{rz}(z; I_0) = \frac{c\pi\rho w_0^2 I_0^n}{n} \left\{ \frac{P\left(\frac{1}{2}, n-2\right)}{(n-2)!} tan^{-1} \left(\frac{z}{z_0}\right) + z \sum_{k=1}^{n-2} \frac{P\left(\frac{1}{2}, n-2\right)(k-1)!}{(n-2)!P\left(\frac{3}{2}, k-1\right)} \frac{1}{\left(1 + \left(\frac{z}{z_0}\right)^2\right)^k} \right\}, \quad (10)$$

for $n \ge 3$, where P(a, b) is the rising factorial, i.e. the Pochhammer polynomial:

$$P(a, b) = a \cdot (a+1) \cdots (a+b-1)$$
. (11)

Eq. (10) represents the signal recorded from a slab with an infinitely large area but with a thickness of z including the origin or the focal position. When $S_{rz}(z; I_0)$ is recorded as a function of I_0 , the result corresponds to a power scan with a slot width z in Fig. 1. Taking the limit of $S_{rz}(z; I_0)$ to $z \to \infty$ should result in the signal from a full-view experiment:

$$S_{FV}(I_0) = \lim_{z \to \infty} S_{rz}(z) = \frac{c\rho \pi^2 w_0^2 I_0^n}{2n} \frac{P(\frac{1}{2'}, n-2)}{(n-2)!} \propto I_0^n , \qquad (12)$$

The above result suggests that for nonlinear processes when the response function can be expressed as a power function of the laser intensity, full-view measurements are not affected by VAE. In hindsight, this conclusion should be expected since the spread of the laser field is throughout the full volume at all intensities, as implied by Eq. (1). Regardless of the laser intensity, the interaction volume never changes, and the sample in the full volume is always in the laser field and contributes to the observation.

These derivations suggest that as long as the response function can be expressed as a power function of the laser intensity, full-view experiments can faithfully reproduce the intensity dependence of a nonlinear process, hence there is no need for spatial filters in the experiment. In other words, the volumetric weighting effect¹⁻⁵ due to increased volume at lower intensities is not a concern when the signal from the full interaction volume can be recorded. Although the condition for Eq. (7) is rarely satisfied, for a qualitative characterization, many experiments still seek the

equivalent value of n within a limited intensity range. Hence this conclusion reassures the measurements of many experiments in the literature on nonlinear processes. $^{10,14-16}$

Fig. 2 shows the sampled volume, 2 the integration kernel, and the response function with n = 6 as a function of the relative intensity $\frac{I}{I_0}$ and $\frac{z}{z_0}$ in a focused laser field with properties defined by Eq. (1). In addition, the percent of ions collected for the corresponding region from $-\frac{z}{z_0}$ to $\frac{z}{z_0}$ is also labeled on the top axis. The response function is scaled by a factor of 20 for visualization. For this highly nonlinear process, most of the signal (94.1%) is produced from the volume defined by $\frac{z}{z_0}$ 1, but the sampled volume only rises substantially when $\frac{z}{z_0} > 1$. This significant volumetric weighting factor favoring the low intensity region is the reason of concern in revealing the true form of the response function. However, for all practical purposes, we can assume that the signal generated in the region with $\frac{z}{z_0} > 2$ (less than 0.2%) can be ignored, meaning that when the intensity is below the corresponding $I_{th} = 0.2I_0$, no ionization event can be detected. At an increased intensity $I_2 = 10I_0$, the volume encompassed by the region with $I > I_{th}$ would increase by 15 folds,² extending to $\frac{z}{z_0} = 7$ and $\frac{r}{w_0} = 2$ based on Eq. (1). If the Rayleigh range is 1 mm, a full-view experiment at I_0 corresponds to a z range of 2 mm, while a full-view experiment at I_2 = $10I_0$ corresponds to a z range of 7 mm.

These numbers define the conditions of a full-view experiment: to qualify as a full-view experiment at intensities ranging from I_0 to $10I_0$, the sample and ion collector need to cover an area with a diameter of 14 mm and a depth of $4w_0$ in the setup of Fig. 1. This dimension requirement for the spectrometer is easily achievable in almost all experimental setups. The spread of the sample, based on the dimensions labeled in Fig. 1, is also reasonable, although it might be

questionable for highly collimated molecular beams. On the other hand, most detectors have a dynamic range less than 6 orders of magnitude, corresponding to an intensity variation of less than one order of magnitude for n = 6. Hence the above assumption of $I_2 = 10I_0$ actually exceeds the range of most realistic experiments, and therefore the real requirement for the dimension of the electrode and beam spread should be smaller.

These conditions for obtaining the correct exponent from a full-view experiment without any spatial discrimination are applicable to highly nonlinear processes away from saturation conditions. With decreasing n, the necessary range of $\frac{z}{z_0}$ expands, so does the corresponding size requirement for the electrodes and beam spread. Moreover, to uncover the saturation conditions of a multiphoton process, i.e. to find the true functional form of R(I), a detailed z-scan experiment and the treatment of Eq. (6) are still necessary.

Non-ideal Gaussian beams

The mode structure of many pulsed lasers, particularly high power Q-switched Nd:YAG lasers, is not well defined, and the beam profile can deviate from Eq. (1), particularly after passing through several non-ideal optical surfaces. We tried to measure the beam properties along both r and z directions using the setup shown in Fig. 3. The laser is a Q-switched Nd:YAG (GCR 230, Spectra Physics) with an oscillator and an amplifier, equipped with a frequency doubling unit to obtain radiation at 532 nm. The maximum pulse energy is 25 mJ with only the oscillator, and 125 mJ with the additional amplification. To obtain pulse energies between 25 and 125 mJ, we can adjust the discharge voltage on the amplifier, or adjust the waveplate on the frequency doubling unit for polarization mismatch. The focal length of the glass lens is 18 cm.

To perform the desired measurements at different pulse energies, however, we need an effective method of reducing the laser power below 1 mJ. This was achieved by reflecting the laser beam from a transparent optical surface, for example, the slanted face of a right angle turning prism. The reflection of < 10% from one surface can reduce the pulse energy from over 100 mJ to a few mJ, and further reflection by another surface results in an energy of ~1 mJ, in the range of easy reading by a standard power meter (SOLO2 (R2), Gentec-EC). To measure the beam width, we initially used a sharp edge made of SiC to cut into the laser beam. During the experiment, however, even with a pulse energy of 1 mJ, the sharp edge was still burnt by the focused laser beam, resulting in large uncertainties. We then changed the sharp edge into a rod of 6 mm in diameter. Although this method is not ideal, the results are consistent over several repeated measurements under the same pulse energies.

The measurement procedure is illustrated in the supplementary document. The transmitted energy is sigmoidal in shape as the rod traverses along the r direction, and differentiation results in a Gaussian function with an equivalent width w(z). Taking these widths as a function of z, we fitted for the equivalent beam waist w_0 and the Rayleigh range z_0 according to Eq. (1).

Table I. Characteristics of the laser beam

	Experiment	Theory
$w_0 (\mu m)$	14.7 ± 6.9	6.0
$z_0 (mm)$	0.7 ± 0.4	0.2

Table I shows the resulting beam waist and Rayleigh range at 25 mJ, together with the theoretical values obtained from the diffraction limit:

$$w_0 = \frac{2f\lambda}{\pi W_a} \,, \tag{13}$$

where W_g is the diameter of the laser beam on the focal lens, and f is the focal length of the lens. We also tried the measurements for pulse energies between 25 and 125 mJ, and the resulting values are consistent with those listed in Table I within the uncertainties. However, these values need to be considered in the following context. The micrometer that controls the motion of the cutter has a smallest division of 10 µm, hence we almost have no means to determine a waist with a theoretical value of 6 µm. The theoretical Rayleigh range is 0.2 mm, which is a more reasonable physical distance for the micrometer. Extrapolation from the experimental Rayleigh range of z_0 = $0.7 \ mm$ results in $w_0 = 11.2 \ \mu m$. This value is within the experimental error of w_0 , and it is also consistent with our repeated measurements at 25 mJ using either a thin blade or a rod as a beam block. We also found that adjusting the pulse energy by the discharge voltage on the flashlamp of the amplifier, or by the orientation of the waveplate in the harmonic generation unit, does not affect the beam parameters, a result not surprising considering the large uncertainty of the reported values. All results reported in this work using different pulse energies were obtained by adjusting the discharge voltage. We acknowledge that every optical surface along the beam propagation direction affects the beam profile, hence the experimental results are only representative of the laser beam after passing through the set of optical surfaces in our experiment, not necessarily representative of the beam directly from the laser.

Multiphoton ionization of Ar

To test the theoretical derivations presented in the above sections, we use multiphoton ionization of Ar as an example. The experimental setup is a standard differentially pumped molecular beam machine as illustrated in Fig. 1, lower right corner, with a pulse valve (General Valve, Series 9, Parker Hannifin, nozzle diameter: 1 mm), and a home-made skimmer of 2 mm in diameter. The stagnation pressure is kept at 1 atm, and no clusters should form when the nozzle is at room

temperature.¹⁷ The time-of-flight mass spectrometer is Wiley-McLaren type,¹⁸ inline with the molecular beam, and the ionization region is sandwiched between the two electrodes of 4.6 cm in diameter. A small tube of 1 mm in diameter and 3 mm in length is mounted upstream from the first electrode, limiting the spread of the molecular beam to ~1 mm in the interaction region, on par with the experimental Rayleigh range of the laser beam. The laser operates at a 10 Hz repetition rate but the sample pulse valve operates at 5 Hz, and the difference in the Ar⁺ signal when the pulse valve is on and off is considered the net signal from the molecular beam. When the laser is fired 0.6 ms after the trigger to the pulse valve, it captures the leading edge of the molecular beam. The resulting measurements, either from z-scan or power-scan, should correspond to ISS experiments. The signal recorded when the pulse valve is off, i.e. the background signal, corresponding to the laser firing 100 ms after the gas pulse, should be from ionization of the residue gas (average vacuum level: 1×10^{-6} torr during operation), essentially unrelated to the molecular beam. This statement has been confirmed by the independence of the background signal on the position of the focal lens along the z-direction: the background signal shows no dependence on the lens position within 2 mm of lens movement. Hence the dependence of the background signal, small as is expected, on the laser power, should correspond to a full-view experiment with no spatial discrimination.

Fig. 4 shows the results of z-scan (labeled "z scan") and power-scan (labeled "P scan") from ISS experiments and from the full-view experiment (labeled "FV") on a log-log plot. The simulation result based on the experimental conditions assuming n = 6 using Eq. (10) is also shown with an extended intensity range (Simu. 2). The traces are shifted in the vertical direction for visualization since only the slope is concerned in this discussion. The numbers in the parentheses are the corresponding slopes from fittings of the data points. In particular, linear regression of the

simulated data in the range of z=0 to 1 mm (Simu. 1) results in a slope of 3.0 ± 0.2 , while regression in the range of z=0 to 2 mm results in a slope of 4.5 ± 0.2 . The first ionization threshold of Ar is at 15.8 eV,¹⁹ requiring 7 photons at 532 nm for ionization, hence we expect n=7 if there is no saturation effect. The z-scan uses the same laser intensity $I_0=1.2 \times 10^{12} \text{W/cm}^2$, and the values of $I_{0L}(z)$ are calculated using the experimental value for z_0 from Table I. The power scan spans a range of pulse energies, and the values of I_0 are also calculated based on the experimental beam waist from Table I.

The resulting slopes from the power scan at 6.0 ± 0.3 and from the full-view experiment at 6.3 ± 0.1 are similar within the experimental uncertainty. The experimental results from z-scan, however, show deviations from a linear relation, although a linear fit still results in a very reasonable quality (coefficient of determination $R^2 = 0.98$) with a slope of 2.8 ± 0.1 . This significant difference in the resulting slope is surprising, but it is faithfully reproduced from the simulation within the same range of z values. Moreover, by extending the dynamic range of z in the simulation, the slope increases and eventually converges to 5.2 when z > 4 mm. Unfortunately, the detection sensitivity of the experiment is limited to less than $2z_0$ in our case, and no Ar+ was detectable when z > 1 mm.

The slopes from the full-view experiment and the power scan are close to the theoretical upper limit of 7, and the value of 6.3 or 6.0 could also be a result of partial saturation, since the last two steps of ionization at 532 nm involve transitions among high Rydberg states of Ar, and some degree of resonant enhancement is possible. The slope from the power scan of the collimated molecular beam is within the error limit of the full-view experiment, but is on the lower side. This trend has proven robust throughout several months of experimental time, and a steady increase in the slope has been observed with increasing delays of the laser. The origin of this

behavior could be attributed to the finite radial range of data collection because of the tube, since Eq. (9) assumes the complete range of r in detection.

The above results confirm the assessment that the conditions for full-view experiments are met in our experiment with the background argon gas even under the highest achievable laser intensities of $1.2 \times 10^{12} \text{W/cm}^2$. The sample is distributed almost uniformly in the ionization region, hence the condition for sample spread is automatically satisfied. The range of intensities is only a factor of 2 (between I_0 and $2I_0$), and the dynamic range of the signal is less than 2 orders of magnitude, hence the effective range of $\frac{z}{z_0}$ is below 3. For this type of highly nonlinear processes, the signal is primarily generated from the volume near the focal position, hence most mass spectrometers have sufficient collection volume to be considered full-view measurements.

The smaller slope near the focal position from the ISS experiment (Fig. 4) is a result of the highly nonlinear dependence of the response signal and the finite diameter of the tube. Fig. 5 shows the effect of tube diameter on the resulting signal and fitting slope. If a smaller tube is used, for example, 0.3 mm in diameter, even within $\frac{z}{z_0} = 0 - 1.25$, the resulting slope is 4.7, almost identical to the slope (5.0) from $\frac{z}{z_0} = 0 - 8$. On the contrary, if the tube is 3 mm in diameter, a flat region between $\frac{z}{z_0} = 0$ and 1.25 is obtained. Linear regression of the region between $\frac{z}{z_0} = 2.5$ and 8 results in a slope of 7.3, a clear deviation from the expected value of 5.0.

This effect of the tube diameter can be understood from the following consideration. In a z-scan experiment, the initial position of the lens aligns the focal point of the laser with the center of the tube. For a large diameter tube, as the lens is shifted, only the outer region near the edge of the tube is affected, but the Rayleigh range is still largely within the tube opening. Since most ions

are generated within the Rayleigh range, the overall signal should not change much at all, until the shift is large enough to cut into the Rayleigh range.

Figs. 4 and 5 reveal an important caveat in performing ISS type experiments: the degree of spatial discrimination and the dynamic range of the recorded data are crucial in revealing the true response function. When the tube diameter is comparable to the Rayleigh range as is the case with the tube of 1 mm in diameter, the dynamic range of z-scan needs to extend to over $2z_0$ to capture the true exponent of the intensity dependence. The smaller the tube diameter, the more reliable the measurement is for the same scanning range. A bigger diameter will not only produce a plateau in z-dependence, but also yield a wrong exponent in the large z region. What is even more alarming is that this plateau could be mistakenly considered a sign of saturation, although it is purely an artifact of insufficient spatial discrimination. In practice, however, a smaller tube diameter results in a smaller signal, and ultimately the detection sensitivity limits the size of the tube. With a tube of 1 mm in diameter, the signal level from our detector has already severely limited the scanning range, leading to a seemingly wrong exponent.

Given the above consideration, one way to alleviate the difficulty of the experiment is to increase the Rayleigh range of the laser beam, by using a lens with a longer focal length or a smaller beam (Eq. 13). However, the available total pulse energy will be the ultimate limiting factor in providing the necessary intensity for the nonlinear effect.

The key for the agreement in Fig. 4 is the knowledge of the waist and Rayleigh range of the laser beam. Without these values, no quantitative agreement can be obtained. However, measurements of beam waists are tedious and time consuming, and require high precision translational stages. If the goal of the experiment is to qualitatively assess exponents of the response function, while the exact value of the exponent is not a major concern, this detailed information can be ignored.

Moreover, if detailed saturation information is deemed unnecessary at a certain stage of investigation, power scans of full-view experiments are sufficient, with no need to perform detailed ISS experiments.

Conclusion

In this report, we investigate the volume average effect in highly nonlinear processes, from simulation and experiment. Our basic conclusion is that when the signal dependence can be expressed as a power function, full-view experiments with sufficiently large collection volumes are adequate for revealing the exponent of the intensity dependence. However, if detailed information on the saturation intensity is desired, ISS experiments with spatial discrimination are needed. We also present a caveat in performing ISS experiments: the degree of spatial discrimination and the corresponding range of *z*-scan have to be taken into consideration when fitting for the exponent. Limited by the dynamic range of detection or the total available laser energy, however, this mission can be challenging. In addition, many nanosecond lasers have mode structures that result in deviations from ideal Gaussian beam profiles, and both values of beam waist and Rayleigh range need to be determined experimentally for quantitative results.

Acknowledgement

This material is based upon work supported by National Science Foundation (1838522).

Supplementary document

Raw data from the translational motion of the beam cutter, differentiation of the raw data to derive the beam width, and fitting of the beam width to obtain the beam waist and Rayleigh range are shown for reference.

Data availability statement

The data that support the findings of this study are available from the corresponding author upon reasonable request.

Figures

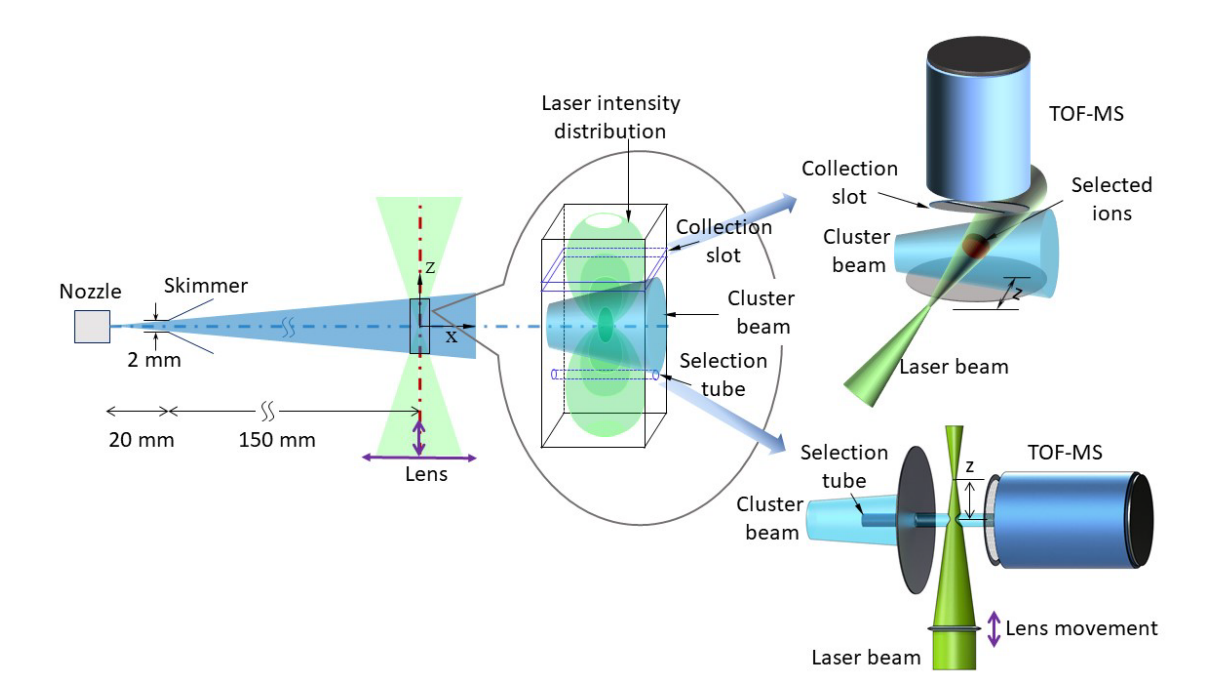


Fig. 1 Experimental setup showing the volume average effect and the two implementations of intensity selective scanning. The top approach uses a slit to select ions with the same z (displacement from the focal position) value, and the bottom approach collimates the molecular beam so its spread is limited to a small range in z. Both methods are called z-scan in the literature.

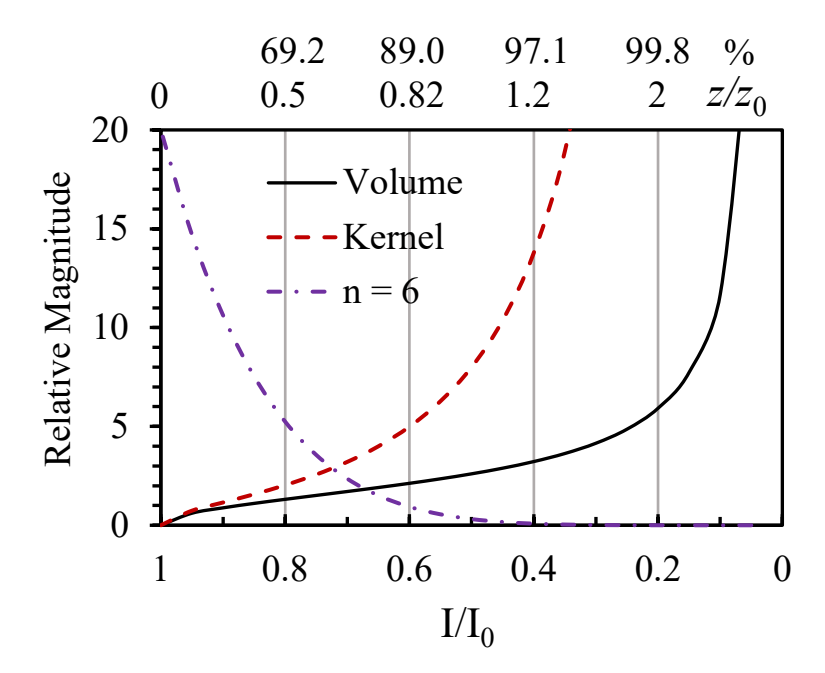


Fig. 2. Dependence of the response function with n=6, volume, and integration kernel on the relative local intensity of the laser and the displacement of the focal position. The response function is scaled by 20 for easy visualization. The "%" label on the top axis represents the percent of total ions within the corresponding values of $-\frac{z}{z_0}$ to $\frac{z}{z_0}$.

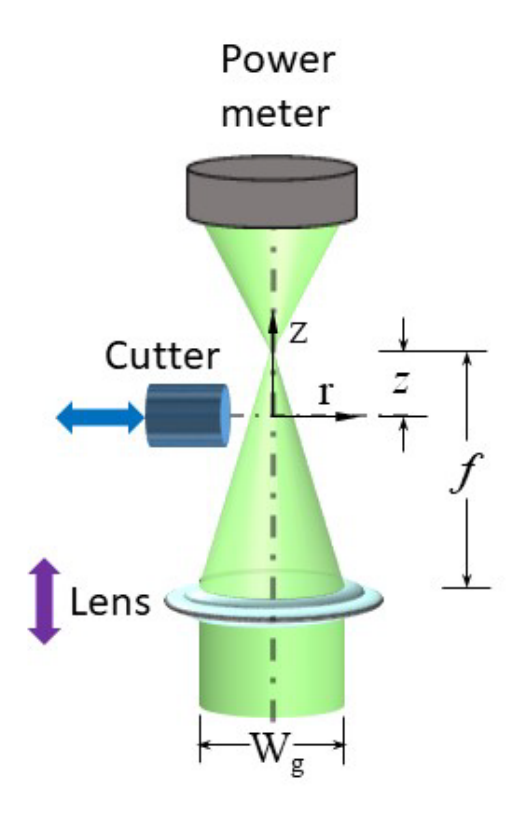


Fig. 3. Experimental setup for measuring the beam waist and Rayleigh range. The cutter and the lens translates along the r and z direction, and the transmitted intensity maps out the beam profile.

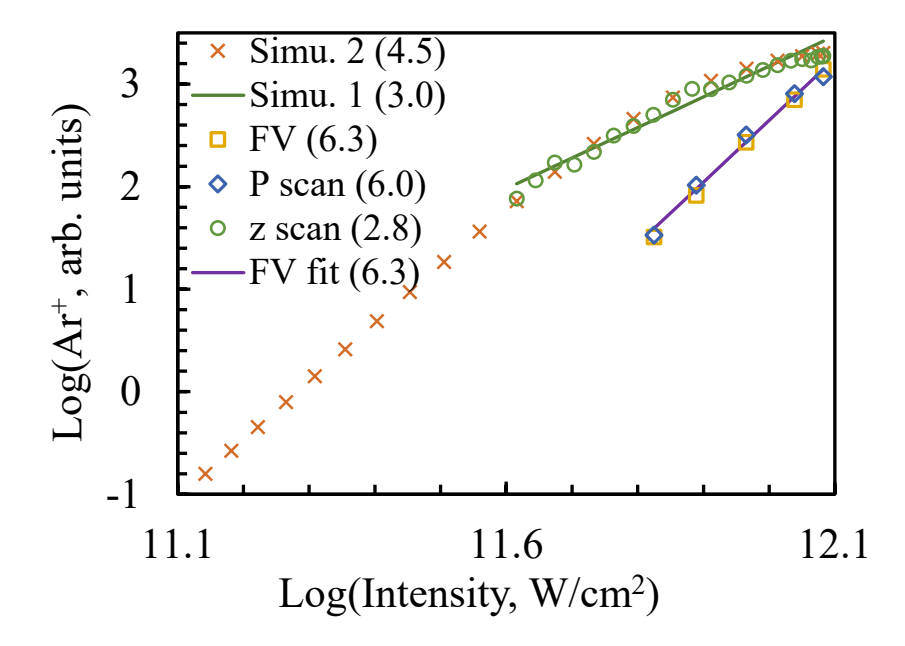


Fig. 4. Experimental results from a full-volume experiment (FV), from z-scan of a collimated molecular beam with a tube of 1 mm in diameter (z scan), from power-scan of the collimated molecular beam (P scan), and from simulations of the experiment (Simu. 2). The numbers in the parentheses are slopes from linear regression fittings. The results from fittings of full-volume (FV fit) and from simulation with z = 0 to 1 mm (Simu. 1) are shown by solid lines.

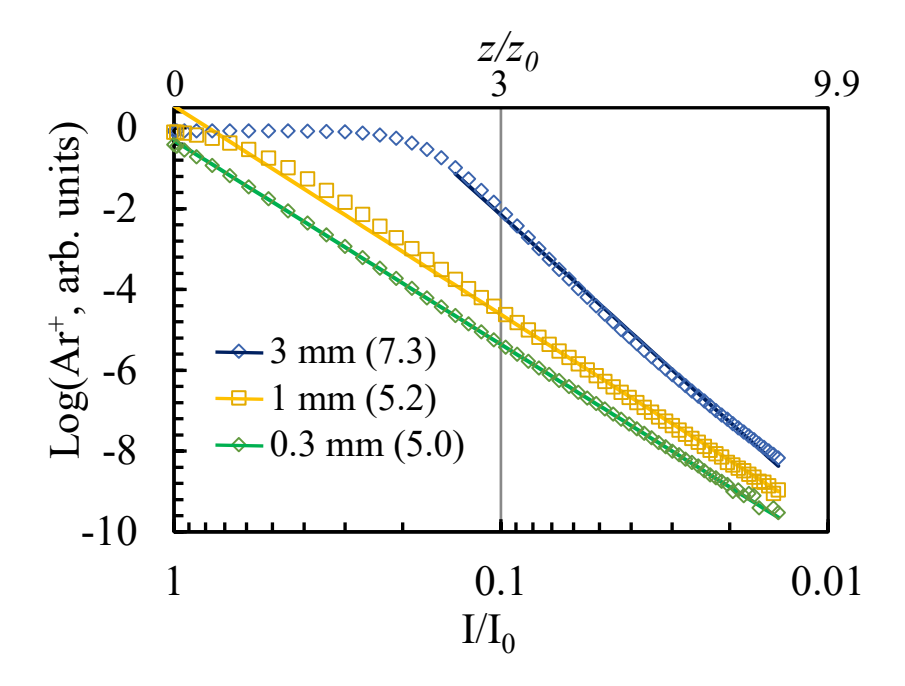


Fig. 5. Effect of tube diameter (labeled in the legend) on the fitting results of the exponents. Open symbols are calculation results assuming n = 6, and continuous lines are results from linear regression, with the corresponding exponents labeled in parentheses. Fittings for tube diameters of 1 and 0.3 mm included all data from $\frac{z}{z_0} = 0 - 8$, but the fitting for the tube of 3 mm in diameter only included the data range between $\frac{z}{z_0} = 2.5 - 8$.

References

- P. Hansch, M. A. Walker, and L. D. Van Woerkom, Phys. Rev. A: At., Mol., Opt. Phys.
 54, R2559 (1996).
- M. A. Walker, P. Hansch, and L. D. Van Woerkom, Phys. Rev. A: At., Mol., Opt. Phys. 57, R701 (1998).
- W. A. Bryan, S. L. Stebbings, J. McKenna, E. M. L. English, M. Suresh, J. Wood, B. Srigengan, I. C. E. Turcu, J. M. Smith, E. J. Divall, C. J. Hooker, A. J. Langley, J. L. Collier, I. D. Williams, and W. R. Newell, Nat. Phys. 2, 379 (2006).
- W. A. Bryan, S. L. Stebbings, E. M. L. English, T. R. J. Goodworth, W. R. Newell, J. McKenna, M. Suresh, B. Srigengan, I. D. Williams, I. C. E. Turcu, J. M. Smith, E. J. Divall, C. J. Hooker, and A. J. Langley, Phys. Rev. A: At., Mol., Opt. Phys. 73, 013407 (2006).
- T. Doeppner, J. P. Mueller, A. Przystawik, J. Tiggesbaeumker, and K. H. Meiwes-Broer, Eur. Phys. J. D **43**, 261 (2007).
- B. Schütte, M. Arbeiter, A. Mermillod-Blondin, M. J. J. Vrakking, A. Rouzee, and T. Fennel, Phys. Rev. Lett. **116**, 033001 (2016).
- T. R. J. Goodworth, W. A. Bryan, I. D. Williams, and W. R. Newell, J. Phys. B: At., Mol. Opt. Phys. 38, 3083 (2005).
- T. Doeppner, J. P. Mueller, A. Przystawik, S. Goede, J. Tiggesbaeumker, K. H. Meiwes-Broer, C. Varin, L. Ramunno, T. Brabec, and T. Fennel, Phys. Rev. Lett. **105**, 053401 (2010).
- ⁹ J. Zhang, Y. Yao, and W. Kong, J. Phys. Chem. Lett. **11**, 1100 (2020).
- ¹⁰ P. Badani, S. Das, P. Sharma, and R. K. Vatsa, Mass Spectrom. Rev. **36**, 188 (2017).
- D. Niu, H. Li, F. Liang, L. Wen, X. Luo, B. Wang, and H. Qu, J. Chem. Phys. **122**, 151103 (2005).
- S. M. Hankin, D. M. Villeneuve, P. B. Corkum, and D. M. Rayner, Phys. Rev. A: At., Mol., Opt. Phys. 64, 013405 (2001).
- ¹³ R. R. Jones, Physical Review Letters **74**, 1091 (1995).
- ¹⁴ S. Das, P. M. Badani, P. Sharma, and R. K. Vatsa, Curr. Sci. **100**, 1008 (2011).
- ¹⁵ N. Zhang, W. Wang, W. Zhao, F. Han, and H. Li, Chem. Phys. **373**, 181 (2010).
- ¹⁶ N. Zhang, W. Wang, H. Cang, H. Wang, and H. Li, Chem. Phys. Lett. **469**, 14 (2009).

- O. F. Hagena and W. Obert, J. Chem. Phys. **56**, 1793 (1972).
- W. C. Wiley and I. H. McLaren, Review of Scientific Instruments 26, 1150 (1955).
- 19 CRC Handbook of Chemistry and Physics, edited by D. R. Lide (CRC Press LLC, Boca Raton, 2004).